

# Quantum Information Processing with Semiconductor Macroatoms

Eliana Biolatti<sup>1,2</sup>, Rita C. Iotti<sup>1,2</sup>, Paolo Zanardi<sup>1,3</sup>, and Fausto Rossi<sup>1,2,3</sup>

<sup>1</sup> *Istituto Nazionale per la Fisica della Materia (INFN)*

<sup>2</sup> *Dipartimento di Fisica, Politecnico di Torino, Corso Duca degli Abruzzi 24, I-10129 Torino,  
Italy*

<sup>3</sup> *Institute for Scientific Interchange (ISI) foundation, Villa Gualino, Viale Settimio Severo 65,  
I-10133 Torino, Italy*

(October 8, 2018)

## Abstract

An *all optical* implementation of quantum information processing with semiconductor macroatoms is proposed. Our quantum hardware consists of an array of semiconductor quantum dots and the computational degrees of freedom are energy-selected interband optical transitions. The proposed quantum-computing strategy exploits exciton-exciton interactions driven by ultrafast sequences of multi-color laser pulses. Contrary to existing proposals based on charge excitations, the present all-optical implementation does not require the application of time-dependent electric fields, thus allowing for a sub-picosecond, i.e. decoherence-free, operation time-scale in realistic state-of-the-art semiconductor nanostructures.

89.70.+c, 03.65.Fd, 73.20.Dx

Typeset using REVTeX

The introduction of quantum information/computation (QIC) [1] as an abstract concept, has given birth to a great deal of new thinking about how to design and realize quantum information processing devices. This goal is extremely challenging: one should be able to perform, on a system with a well-defined quantum state space (the *computational* space), precise quantum-state preparation, coherent quantum manipulations (*gating*) of arbitrary length, and state detection as well. It is well known that the major obstacle to implement this ideal scheme is *decoherence*: the spoiling of the unitary character of quantum evolution due to the uncontrollable coupling with environmental, i.e., non-computational, degrees of freedom. Mostly due to the need of low decoherence rates, the first proposals for experimental realizations of quantum information processing devices originated from specialties in atomic physics [2], in quantum optics [3], and in nuclear and electron magnetic-resonance spectroscopy [4]. On the other hand, practically relevant quantum computations require a large number of quantum-hardware units (*qubits*), that are known to be hardly achievable in terms of such systems. In contrast, in spite of the serious difficulties related to the “fast” decoherence times, a solid-state implementation of QIC seems to be the only way to benefit synergistically from the recent progress in ultrafast optoelectronics [5] as well as in meso/nanostructure fabrication and characterization [6]. Among the proposed solid-state implementations one should mention those in superconducting device physics [7] and in meso- and nanoscopic physics [8]. In particular, the first semiconductor-based proposal, by Loss and DiVincenzo, relies on spin dynamics in quantum dots; it exploits the low decoherence of spin degrees of freedom in comparison to the one of charge excitations.

As originally envisioned in [9], gating of charge excitations could be performed by exploiting *present* ultrafast laser technology [5], that allows to generate and manipulate electron-hole quantum states on a sub-picosecond time-scale: *coherent-carrier-control* [10]. In this respect, decoherence times on nano/microsecond scales can be regarded as “long” ones. Based on this idea a few implementations have been recently put forward [11]; However, while in these proposals single-qubit operations are implemented by means of ultrafast optical spectroscopy, the control of two-qubit operations still involves the application of external

fields and/or microcavity-mode couplings, whose switching times are much longer than decoherence times in semiconductor quantum dots (QDs). It clearly follows that such proposals are currently out of reach in terms of state-of-the-art optoelectronics technology.

As already pointed out in [9], in order to take full advantage from modern ultrafast laser spectroscopy one should be able to design fully optical gating schemes able to perform single- and two-qubit operations on a sub-picosecond time-scale. Following this spirit, in this Letter we propose the first *all-optical* implementation with semiconductor macromolecules. Our analysis is based on a realistic, fully three-dimensional, description of multi-QD structures, whose many-body electron-hole Hamiltonian can be schematically written as [12]:

$$\mathbf{H} = \mathbf{H}_o + \mathbf{H}' = (\mathbf{H}_c + \mathbf{H}_{cc}) + (\mathbf{H}_{cl} + \mathbf{H}_{env}) , \quad (1)$$

where  $\mathbf{H}_c$  describes the non-interacting electron-hole system within the nanostructure confinement potential,  $\mathbf{H}_{cc}$  is the sum of the three (electron-electron, hole-hole, and electron-hole) Coulomb-interaction terms,  $\mathbf{H}_{cl}$  describes the coupling of the carrier system with a classical light field [13], while  $\mathbf{H}_{env}$  describes the interaction of the carrier system with environmental degrees of freedom, like phonon and plasmon modes of the host material. The latter is responsible for decoherence processes and it will be accounted for within a density-matrix formalism (see below).

For any given number of electron-hole pairs  $N$ , a direct diagonalization of  $\mathbf{H}_o$  will provide the many-body states of the interacting electron-hole system; they, in turn, allow to evaluate many-exciton optical spectra, i.e., the absorption probability corresponding to the generic  $N \rightarrow N'$  transition.

The above theoretical scheme has been applied to realistic state-of-the-art QD arrays. In particular, as quantum hardware, we consider a GaAs-based structure with in-plane parabolic confinement potential [14]; Moreover, as discussed below (see Fig. 2), in order to induce a significant exciton-exciton dipole coupling, an in-plane static electric field  $F$  is applied. The square-like carrier confinement along the growth ( $z$ ) direction for electrons and holes is schematically depicted in Fig. 1 for the array unit cell  $a + b$ . We stress that

the geometrical and material parameters of the proposed prototypical structure in Fig. 1 are fully compatible with current QD growth and characterization technology [6,10].

Let us discuss first the optical response of the *semiconductor macromolecule* ( $a + b$ ) in Fig. 1. The excitonic ( $0 \rightarrow 1$ ) optical spectrum in the presence of an in-plane electric field  $F = 15 \text{ kV/cm}$  is shown in Fig. 2(A), where the two lowest optical transitions correspond to the formation of direct ground-state excitons in dot  $a$  and  $b$ , respectively (see Fig. 1). In contrast, the high-energy peaks correspond to optical transitions involving excited states of the in-plane parabolic potential. Due to the strong in-plane carrier confinement, the low-energy excitonic states are expected to closely resemble the corresponding single-particle ones, thus involving the parabolic-potential ground state only. This is confirmed by the excitonic spectrum (solid curve) in Fig. 2(B), which has been obtained limiting our single-particle basis set to the parabolic-potential ground state. As we can see, apart from a small rigid shift, the relative position of the lowest transitions is the same. This suggests to use as a basis of our computational space the set formed by the lowest excitonic transition in each QD.

Let us now come to the biexcitonic spectrum [dashed line in Fig. 2(B)]; it describes the generation of a second electron-hole pair in the presence of a previously created exciton ( $1 \rightarrow 2$  optical transitions). The crucial feature in Fig. 2(B) is the magnitude of the "biexcitonic shift" [6], i.e., the energy difference between the excitonic and the biexcitonic transition (see solid and dashed curves). For the QD structure under investigation we get energy splittings up to 5 meV [see inset in Fig. 2(B)], which is by far larger than typical biexcitonic splittings in single QDs [6]. This is due to the in-plane static field  $F$ , which induces a charge separation between electrons and holes. This, in turn, gives rise to significant dipole-dipole coupling between adjacent excitonic states. The microscopic origin of such exciton-exciton coupling is the same of the Forster process exploited by Quiroga and Johnson [15] for the generation of entangled states in coupled QDs.

The physical origin of the biexcitonic shift  $\Delta\mathcal{E}$  is qualitatively described in Fig. 2(C), where we show the electron and hole charge distribution corresponding to the biexcitonic

ground state.

The central idea in our QIC proposal is to exploit such few-exciton effect to design *conditional operations*. To this end let us introduce the excitonic occupation number operators  $\hat{n}_l$ , where  $l$  denotes the generic QD in our array. The two states with eigenvalues  $n_l = 0$  and  $n_l = 1$  correspond, respectively, to the absence (no conduction-band electrons) and to the presence of a ground-state exciton (a Coulomb-correlated electron-hole pair) in dot  $l$ ; they constitute our single-qubit basis:  $|0\rangle_l$  and  $|1\rangle_l$ . The whole computational state-space  $\mathcal{H}$  is then spanned by the basis  $|\mathbf{n}\rangle = \otimes_l |n_l\rangle$ , ( $n_l = 0, 1$ ).

The full many-body Hamiltonian  $\mathbf{H}_o$  in (1) restricted to the above computational space  $\mathcal{H}$  reduces to

$$\tilde{\mathbf{H}}_o = \sum_l \mathcal{E}_l \hat{n}_l + \frac{1}{2} \sum_{ll'} \Delta\mathcal{E}_{ll'} \hat{n}_l \hat{n}_{l'}. \quad (2)$$

Here,  $\mathcal{E}_l$  denotes the energy of the ground-state exciton in dot  $l$  while  $\Delta\mathcal{E}_{ll'}$  is the biexcitonic shift due to the Coulomb interaction between dots  $l$  and  $l'$ , previously introduced (see Fig. 2). The effective Hamiltonian in (2) has exactly the same structure of the one proposed by Lloyd in his pioneering paper on quantum cellular automata [16], and it is the Model Hamiltonian currently used in most of the NMR quantum-computing schemes [17]. This fact is extremely important since it tells us that: (i) the present semiconductor-based implementation contains all relevant ingredients for the realization of basic QIC processing; (ii) it allows to establish a one-to-one correspondence between our semiconductor-based scheme and much more mature implementations, like NMR [17].

According to (2), the single-exciton energy  $\mathcal{E}_l$  is renormalized by the biexcitonic shift  $\Delta\mathcal{E}_{ll'}$ , induced by the presence of a second exciton in dot  $l'$  ( $\tilde{\mathcal{E}}_l = \mathcal{E}_l + \sum_{l' \neq l} \Delta\mathcal{E}_{ll'} n_{l'}$ ). In order to better illustrate this idea, let us focus again on the two-QD structure, i.e. two-qubit system, of Fig. 1 and fix our attention on one of the two dots, say dot  $b$ . The effective energy gap between  $|0\rangle_b$  and  $|1\rangle_b$  depends now on the occupation of dot  $a$ . This elementary remark suggests to design properly tailored laser-pulse sequences to implement controlled-not logic gates among the two QDs as well as single-qubit rotations. Indeed, by sending an ultrafast

laser  $\pi$ -pulse with central energy  $\hbar\omega_b[n_a] = \mathcal{E}_b + \Delta\mathcal{E}_{ba}n_a$ , the transition  $|n_b\rangle_b \rightarrow |1 - n_b\rangle_b$  ( $\pi$ -rotation) of the *target* qubit (dot  $b$ ) is obtained if and only if the *control* qubit (dot  $a$ ) is in the state  $|n\rangle_a$ . Notice that the above scheme corresponds to the so-called selective population transfer in NMR [17]; alternative procedures used in that field can be adapted to the present proposal as well.

Moreover, by denoting with  $U_b^{n_a}$  the generic unitary transformation induced by the laser  $\pi$ -pulse of central frequency  $\omega_b[n_a]$ , it is easy to check that the two-color pulse sequence  $U_b^0 U_b^1$  achieves the unconditional  $\pi$ -rotation of qubit  $b$ .

In order to test the viability of the proposed quantum-computation strategy, we have performed a few simulated experiments of basic quantum information processing. Our time-dependent simulations are based on the realistic state-of-the-art QD structure of Fig. 1:  $\mathcal{E}_a = 1.70$  eV,  $\mathcal{E}_b = 1.71$  eV,  $\Delta\mathcal{E} = 4, 5$  meV, which correspond to  $F = 30$  kV/cm [see inset in Fig. 2(B)]. They are based on a numerical solution of the Liouville-von Neumann equation describing the exact quantum-mechanical evolution of the many-exciton system (2) within our computational subspace  $\mathcal{H}$  in the presence of environment-induced decoherence processes [see term  $\mathbf{H}_{env}$  in Eq. (1)] [18]. Figure 3 shows a simulated sequence of single- plus two-qubit operations driven by a two-color laser-pulse sequence.

Initially the system is in the state  $|0, 0\rangle \equiv |0\rangle_a \otimes |0\rangle_b$ . The first laser pulse (at  $t = 0.2$  ps) is tailored in such a way to induce a  $\frac{\pi}{2}$  rotation of the qubit  $a$ :  $|0, 0\rangle \rightarrow (|0, 0\rangle + |1, 0\rangle)/\sqrt{2}$ . At time  $t = 0.8$  ps a second pulse induces a conditional  $\pi$ -rotation of the qubit  $b$ :  $|0, 0\rangle + |1, 0\rangle \rightarrow |0, 0\rangle + |1, 1\rangle$ . This last operation plays a central role in any quantum information processing, since it transforms a *factorized* state ( $(|0\rangle + |1\rangle) \otimes |0\rangle$ ) into an *entangled* state. The scenario described so far is confirmed by the time evolution of the exciton occupation numbers  $n_a$  and  $n_b$  reported in (A) as well as of the diagonal elements of the density matrix (in our four-dimensional computational basis) reported in (B). As we can see, during the pulse energy-nonconserving (or off-resonant) transitions [12] take place; however, at the end of the pulse such effects vanish and the desired quantum state is reached.

The experiment simulated above clearly shows that the energy scale of the biexcitonic

splitting in our quantum-dot molecule [see Fig. 2] is compatible with the sub-picosecond operation time-scale of Fig. 3.

At this point a few comments are in order. First we stress a very important feature of the proposed semiconductor-based implementation: as for NMR quantum computing, two-body interactions are always switched on (this should be compared to the schemes in which two-qubit gates are realized by turning on and off the coupling between subsystems, e.g., by means of slowly-varying fields and cavity-mode couplings); conditional as well as unconditional dynamics is realized by means of sequences of ultrafast single-qubit operations whose length does not scale as a function of the total number of QDs in the array [19].

Let us now come to the *state measurement*. In view of the few-exciton character of the proposed quantum hardware, the conventional measurement of the carrier subsystem by spectrally-resolved luminescence needs to be replaced by more sensitive detection schemes. To this end, a viable strategy could be to apply to our semiconductor-based structure the well-known recycling techniques commonly used in quantum-optics experiments [20]. Generally speaking, the idea is to properly combine quantum- and dielectric-confinement effects in order to obtain well-defined energy levels, on which to design energy-selective photon-amplification schemes.

The nanoscale range of the inter-dot coupling we employed for enabling conditional dynamics does not allow for space-selective optical addressing of individual qubits. For this reason, at least for our basic QD molecule ( $a+b$ ), we resorted to an energy selective addressing scheme. However, extending such strategy to the whole QD array would imply different values of the excitonic transition in each QD, i.e.,  $\mathcal{E}_l \neq \mathcal{E}_{l'}$ . This, besides obvious technological difficulties, would constitute a conceptual limitation of scalability towards massive Quantum Computations. The problem can be avoided following a completely different strategy originally proposed by Lloyd [16] and recently improved in [21]: by properly designed sequences of multicolor global pulses within a cellular-automaton scheme, local addressing is replaced by information-encoding transfer along our QD array.

Finally, a present limitation of the proposed quantum hardware are the non-uniform

structural and geometrical properties of the QDs in the array, which may give rise to energy broadenings larger than the biexcitonic shift. However, recent progress in QD fabrication—including the realization of QD structures in microcavities— will allow, we believe, to overcome this purely technological (non conceptual) limitation.

In summary, the first *all optical implementation of QIC with a semiconductor-based quantum hardware* has been proposed. Our analysis has shown that energy-selected optical transitions in realistic state-of-the-art QD structures are good candidates for quantum-information encoding and manipulation. The sub-picosecond time-scale of ultrafast laser spectroscopy allows for a relatively large number of elementary operations within the exciton decoherence time.

We are grateful to David DiVincenzo, Neil Johnson, Seth Lloyd, and Mario Rasetti for stimulating and fruitful discussions.

This work has been supported in part by the European Commission through the Research Project *SQID* within the *Future and Emerging Technologies (FET)* programme.



## REFERENCES

- [1] See, e.g., D.P. DiVincenzo and C. Bennet, *Nature* **404**, 247 (2000) and references therein.
- [2] J.I. Cirac and P. Zoller, *Phys. Rev. Lett.* **74**, 4091 (1995); T. Pellizzari *et al.*, *Phys. Rev. Lett.* **75**, 3788 (1995); C. Monroe *et al.*, *Phys. Rev. Lett.* **75**, 4714 (1995); A. Sorensen and K. Molmer, *Phys. Rev. Lett.* **82**, 1971 (1999).
- [3] Q.A. Turchette *et al.*, *Phys. Rev. Lett.* **75**, 4710 (1995); A. Imamoglu *et al.*, *Phys. Rev. Lett.* **83**, 4204 (1999).
- [4] N. Gershenfeld and I. Chuang, *Science* **275**, 350 (1997)
- [5] See, e.g., J. Shah, *Ultrafast Spectroscopy of Semiconductors and Semiconductor Nanostructures* (Springer, Berlin, 1996).
- [6] See, e.g., L. Jacak, P. Hawrylak, A. Wojs, *Quantum Dots* (Springer, Berlin, 1998).
- [7] A. Shnirman *et al.*, *Phys. Rev. Lett.* **79**, 2371 (1997); J.E. Mooij *et al.*, *Science* **285**, 1036 (1999).
- [8] D. Loss and D.P. DiVincenzo, *Phys. Rev.A* **57**, 120 (1998); B. Kane, *Nature* **393**, 133 (1998).
- [9] P. Zanardi and F. Rossi, *Phys. Rev. Lett.* **81**, 4752 (1998).
- [10] N.H. Bonadeo *et al.*, *Science* **282**, 1473 (1998).
- [11] M. Sherwin *et al.*, *Phys. Rev.A* **60**, 3508 (1999); T. Tanamoto, *Phys. Rev.A* **61**, 22305 (2000).
- [12] F. Rossi, topical review on *Coherent phenomena in semiconductors*, *Semicond. Sci. Technol.* **13**, 147 (1998).
- [13] The carrier-light (cl) coupling term is responsible for the creation/recombination of electron-hole pairs and it will induce the desired single-qubit rotations.

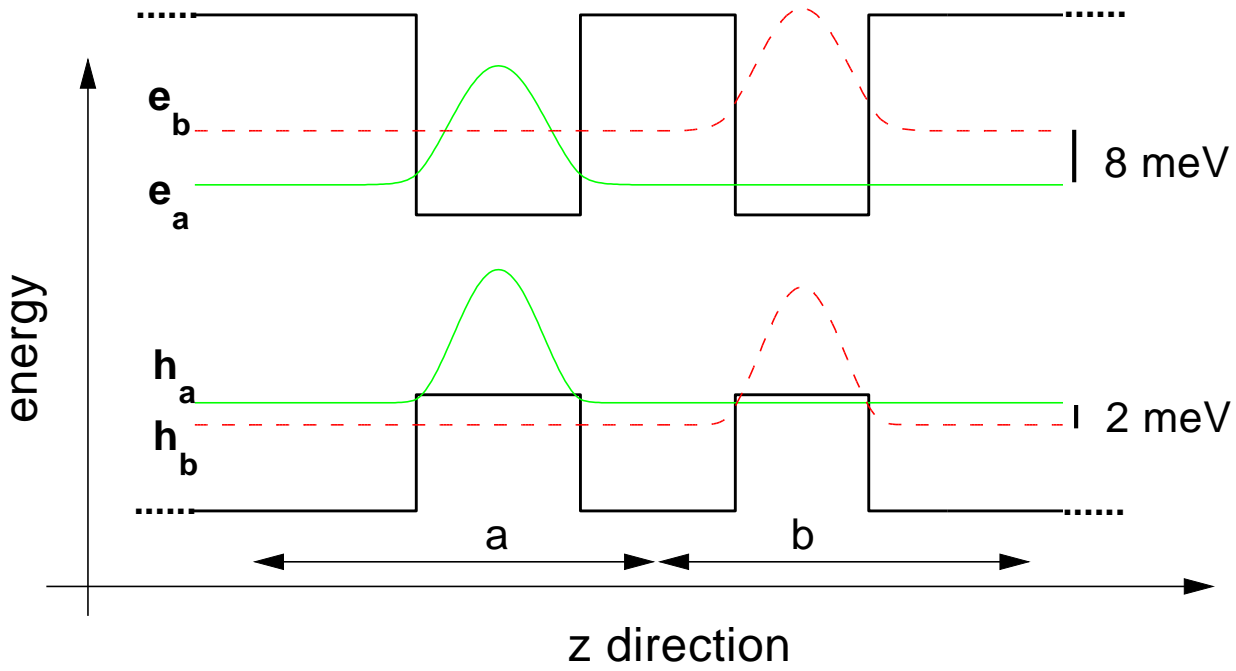
- [14] The interlevel energy splitting of the in-plane parabolic potential has been chosen to be 30 meV for electrons and 16 meV for holes.
- [15] L. Quiroga and N.F. Johnson, Phys. Rev. Lett. **83**, 2270 (1999).
- [16] S. Lloyd, Science **261**, 1569 (1993).
- [17] D.G. Cory *et al.*, Preprint quant-ph/0004104 at <http://xxx.lanl.gov> (2000).
- [18] Decoherence processes are accounted for in our density-matrix formalism by means of a standard  $T_1T_2$  model: we employ a band-to-band recombination time  $T_1 = 1$  ns and we describe phonon-induced decoherence processes in terms of an exciton-phonon dephasing time  $T_2 = 50$  ps, which is compatible with the experimental values given in [10].
- [19] Due to the short-range nature of the exciton-exciton dipole interaction, we are allowed to consider nearest-neighbor coupling only: indeed, for the specific quantum hardware considered (see Fig. 1), in view of the  $\frac{1}{r^3}$  behaviour and, more important, of their small oscillator strengths, second-neighbor couplings play no significant role.
- [20] Q.A. Turchette *et al.*, Phys. Rev.A **61**, 63418 (2000).
- [21] S.C. Benjamin, Phys. Rev.A **61**, 20301 (2000).

## FIGURES

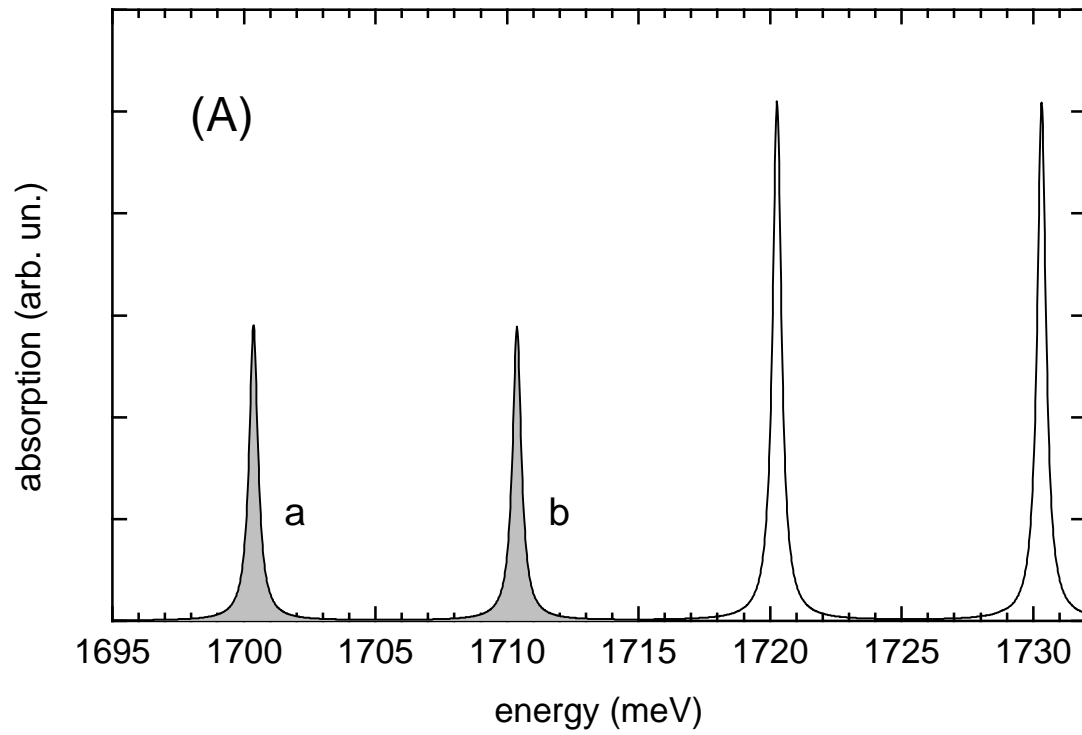
FIG. 1. Schematic representation of the square-like potential profile for electrons (e) and holes (h) along the growth ( $z$ ) direction of our QD array. This is tailored in such a way to allow for an energy-selective creation/destruction of bound electron-hole pairs (i.e., excitons) in dots  $a$  and  $b$ . Moreover, the inter-dot barrier width ( $w \sim 50 \text{ \AA}$ ) is such to prevent single-particle tunneling and at the same time to allow for significant inter-dot Coulomb coupling.

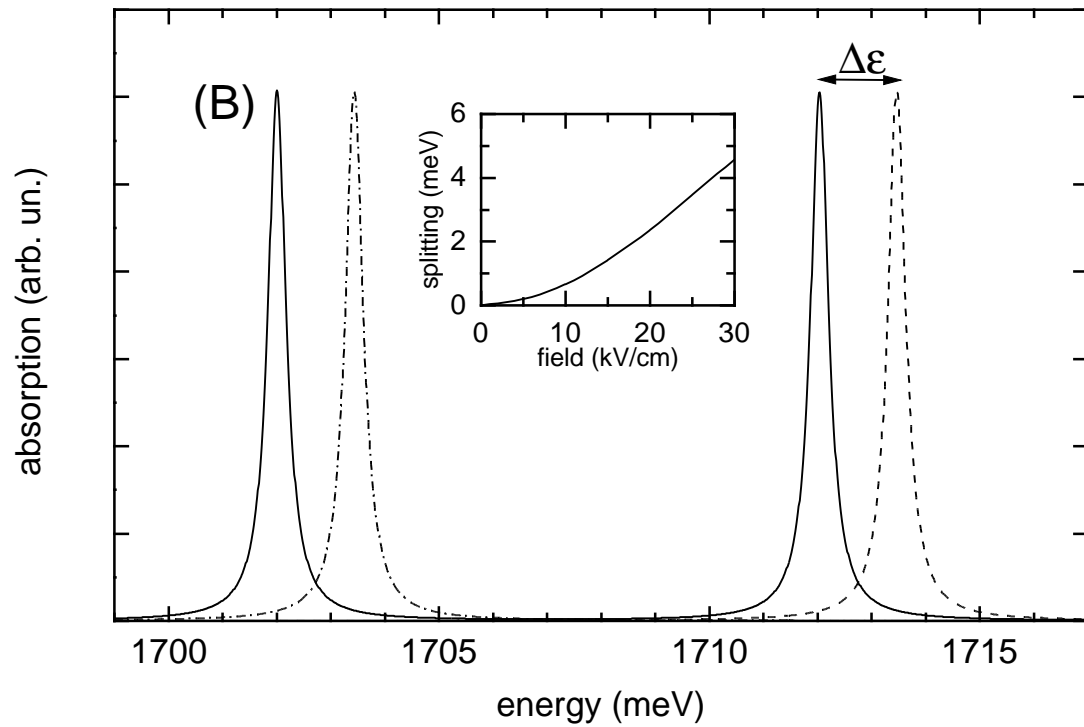
FIG. 2. Optical response of the array unit cell ( $a+b$ ) in Fig. 1. (A) Excitonic spectrum obtained including the realistic multilevel structure of the in-plane parabolic potential. (B) Excitonic (solid curve) and biexcitonic spectrum (dashed curve) obtained including the in-plane ground state only. Due to the well-defined polarization of our laser source, the two structures in the biexcitonic spectrum correspond to the formation of an exciton in dot  $a$  given an exciton in dot  $b$  and *vice versa*. (C) Three-dimensional view of the spatial charge distributions of the two electrons ( $e_a$  and  $e_b$ ) and holes ( $h_a$  and  $h_b$ ) corresponding to the biexcitonic ground state in (B). As we can see, the charge separation induced by the static field increases significantly the average distance between electrons and holes, thus decreasing their attractive interaction. On the other hand, the repulsive terms are basically field independent. This is the origin of the positive energy difference  $\Delta\mathcal{E}$  in (B).

FIG. 3. Time-dependent simulation of single (unconditional) plus two-qubit (conditional) operations (see text). (A) Exciton populations ( $n_a$  and  $n_b$ ), and (B) diagonal elements of the density matrix as a function of time. The two-color pulse sequence is also sketched schematically.

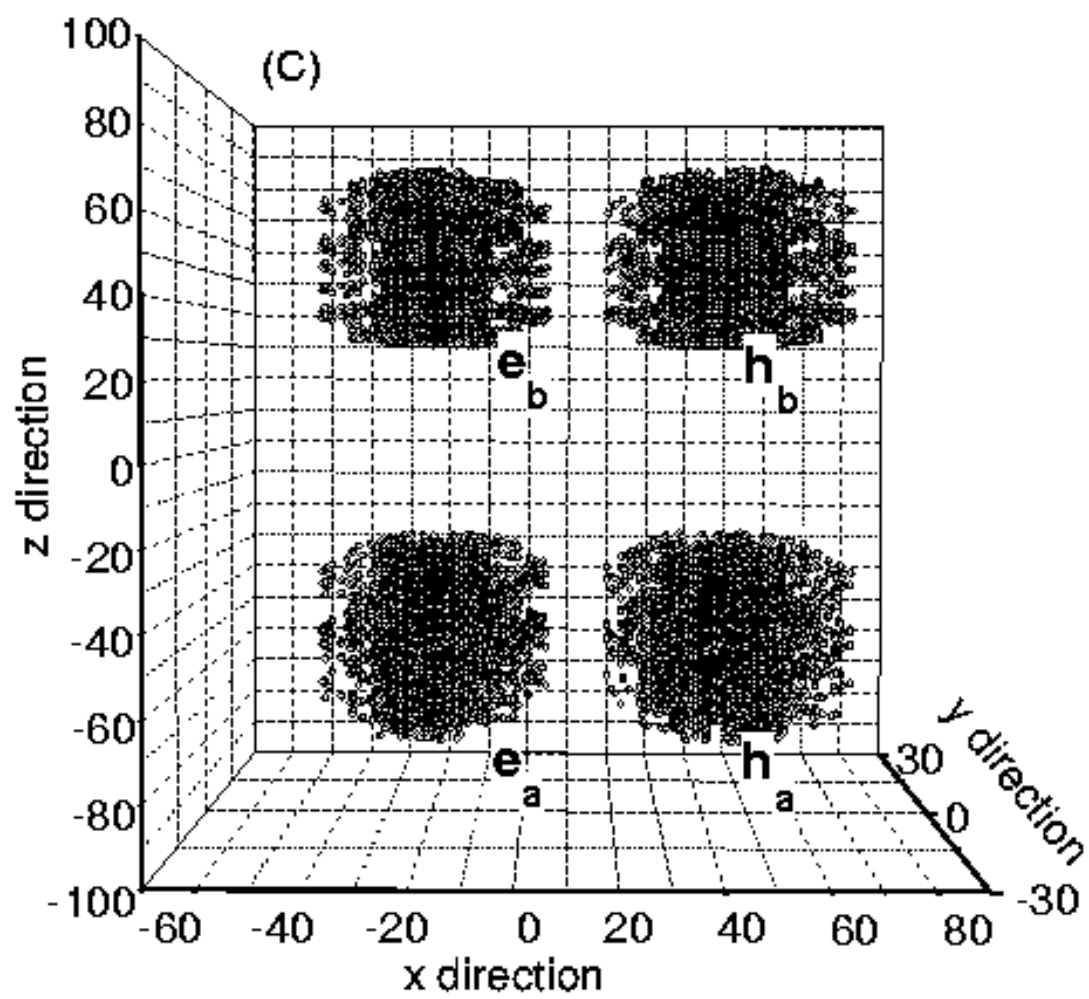


E. Biolatti et al., figure 1

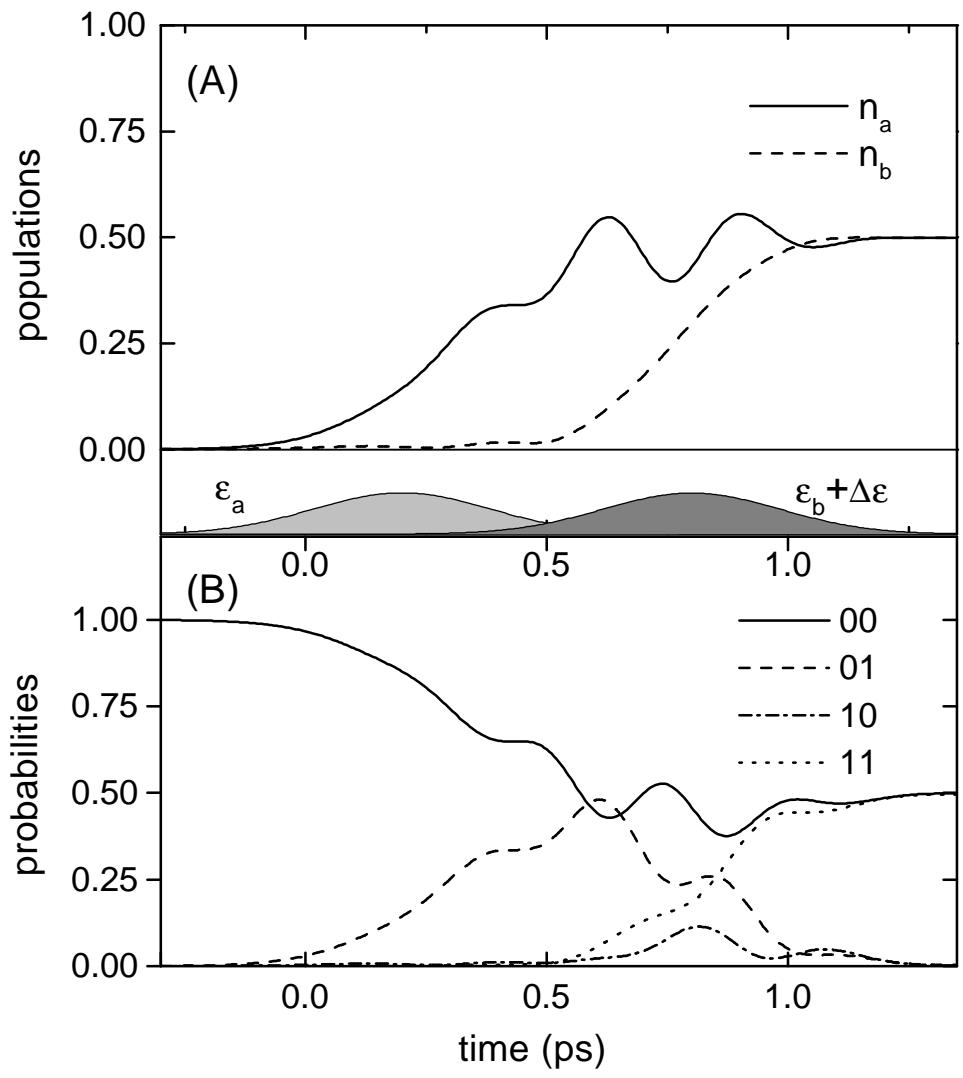




E. Biolatti et al., figure 2B



E. Biolatti et al., figure 2C



E. Biolatti et al., figure 3